Concerted Influence of Key Amino Acids on the Lipid Binding Properties of a Single-Spanning Membrane Protein: NMR and Mutational Analysis

Florence Mousson,[‡] Veronica Beswick,[‡,§] Yves-Marie Coïc,[||] Françoise Baleux,[||] Tam Huynh-Dinh,[||] Alain Sanson,[‡,⊥] and Jean-Michel Neumann*[,‡]

Biophysique des Protéines et des Membranes, CEA DSV/DBCM and URA CNRS 2096, Centre d'Etudes de Saclay, 91191 Gif sur Yvette Cedex, France, and Unité de Chimie Organique, URA CNRS 487, Institut Pasteur, 28 rue du Dr Roux, 75724 Paris, France

Received May 7, 2001; Revised Manuscript Received June 20, 2001

ABSTRACT: Finding the combinations of key amino acids involved in the interaction network underlying the interfacial features of membrane proteins would contribute to a better understanding of their sequence−structure−function relationships and the role of anionic phospholipids. To further address these questions, we performed mutational analysis associated with NMR experiments on synthetic fragments of the single-spanning membrane protein PMP1 that exhibit binding specificity for phosphatidylserine (PS). The aromatic and glutamine residues of the helix part of the PMP1 cytoplasmic domain were mutated. ^{1}H NMR experiments were carried out using perdeuterated DPC micelles as a membrane-like environment, in the absence and presence of small amounts of either POPC or POPS lipids. From intermolecular NOEs and chemical shift data, specific and nonspecific aspects of peptide−phospholipid interactions were distinguished. The major finding of our study is to reveal the concerted influence of a tryptophan and a glutamine residue on the interfacial conformation and lipid binding specificity of the PMP1 cytoplasmic domain.

Understanding the molecular basis governing the lipid−membrane protein interactions requires structural details at atomic resolution. With regard to intrinsic proteins, available data are rather scarce (*1*−*5*). In particular, little is known about the interaction networks conferring binding specificity for anionic phospholipids, apart from the obvious implication of basic side chains. Such a specificity directly concerns the membrane interface, an environment that may promote conformational characteristics and positioning of extra- and transmembrane domains of intrinsic proteins. One can thus wonder about the possible concerted implication of key amino acids in these interfacial features. Recent results obtained in our laboratory led us to consider fragments of the single-spanning membrane protein PMP1 as convenient candidates for exploring the molecular mechanisms underlying the overall lipid−peptide interaction network.

PMP1 is a small membrane protein functioning as a regulatory subunit of the yeast H^+-ATPase (*6*, *7*). Its C-terminal cytoplasmic domain, corresponding to bold residues in the sequence given below, is highly positively charged:

L_1-P-G-G-V_5-I-L-V-F-I_{10}-L-V-G-L-A_{15}-C-I-A-I-I_{20}-A-T-I-I-**Y_{25}-R-K-W-Q-A_{30}-R-Q-R-G-L_{35}-Q-R-F_{38}**

^{1}H NMR[1] experiments have shown that the PMP1 A18−F38 fragment, solubilized in perdeuterated DPC-d_{38} micelles, adopts a single-helix conformation extending from the N-terminus up to Q32 (*8*). The N-terminal helix thus includes the truncated hydrophobic A18−I24 segment and a part of the charged cytoplasmic domain, Y25−Q32. The C-terminal extremity, R33−F38, folds back toward the micelle interior (*9*). As a result, the PMP1 fragment exhibits a ringlike interfacial distribution of five basic side chains and has been shown by ^{2}H NMR to specifically bind POPS when inserted in mixed POPC/POPS bilayers (*10*). In summary, PMP1 provides an exemplary short sequence that exhibits identified conformational and lipid binding features. Mutational analysis associated with NMR experiments should provide relevant insight into the combination of key amino acids that encodes these properties.

With this view, we report here on the ^{1}H NMR studies of the PMP1 G13−F38 fragment and four mutants. The choice of the G13−F38 peptide (70% of the whole PMP1 sequence), instead of the shorter fragment (A18−F38) previously studied, was made to strengthen the stability of the N-terminal helix and the stability of the lipid−peptide complexes. Satisfactorily, the chemical synthesis of the G13−F38 fragments provides the yield and degree of purity required for NMR experiments. The mutational analysis

* To whom correspondence should be addressed. Fax: 33 1 69 08 81 39. E-mail: neumann@dsvidf.cea.fr.

‡ CEA DSV/DBCM and URA CNRS 2096.

§ Current address: Université d'Evry, Bd F. Mitterrand, 91025 Evry, France.

|| Institut Pasteur.

⊥ Current address: Université P. & M. Curie, 9 quai Saint-Bernard, Bât C, 75005 Paris, France.

[1] Abbreviations: DPC, dodecylphosphocholine; MPLC, medium-pressure liquid chromatography; NMR, nuclear magnetic resonance; NOESY, nuclear Overhauser enhancement spectroscopy; POPC, 1-palmitoyl-2-oleoyl-3-glycerophosphatidylcholine; POPS, 1-palmitoyl-2-oleoyl-3-glycerophosphatidylserine; TFA, trifluoroacetic acid; TOCSY, total correlated spectroscopy.

10.1021/bi010924e CCC: $20.00
Published on Web 07/27/2001

concerns the aromatic and glutamine residues of the helix part of the cytoplasmic domain, i.e., Y25, W28, Q29, and Q32. This choice was made for the following reasons.

The influence of Trp and Tyr residues on the interfacial positioning of membrane proteins has been clearly established (*11*−*13*) and, in the case of PMP1, assigned to those of the amphiphilic helix motif, Y_{25}-R-K-W_{28} (*8*). In the context evoked above, we first investigated the extent to which Y25 and W28 substitutions affect both the conformational features of the PMP1 fragment (G13−F38) and its lipid binding specificity for POPS. We then focused on the influence of Q29 and Q32 because (i) they are spatially close to Y25 and W28, respectively, in a helix structure and (ii) from preliminary docking simulations their side chains, acting as both H-bond donor and acceptor groups, are predicted to markedly contribute with the basic residues to the PMP1−POPS interaction network. Hence, the PMP1 fragment (G13−F38) and its four mutants (Y25L, W28L, Q29S, and Q32S) were synthesized. Their conformational and lipid binding properties were investigated using ^{1}H NMR.

Standard two-dimensional ^{1}H NMR experiments were performed using perdeuterated DPC micelles as a membrane-like environment, in the absence and presence of small amounts of protonated POPC and POPS lipids. The relevance of DPC micelles for studying structural and lipid binding properties of membrane protein fragments or domains, initially used by Lauterwein et al. (*14*), has been further assessed by numerous works (for an extensive review, see ref *15*) and in particular by several recent studies (*16*−*20*). The choice of POPC/POPS lipids results from our previous ^{2}H NMR study already mentioned (*10*) and from the presence of an *sn-2* double bond that provides ^{1}H NMR signals probing the middle position of the oleoyl chain (*21*). The lipid binding properties of the PMP1 fragments were studied by analyzing the peptide−lipid intermolecular NOEs and the chemical shift effects observed on both the peptide and lipid proton signals.

MATERIALS AND METHODS

Peptide Synthesis and Purification. Peptides were synthesized by using continuous-flow Fmoc/tBu chemistry (*22*−*24*) on an Applied Biosystems (Foster City, CA) Pioneer peptide synthesizer. All chemical reagents were purchased from Applied Biosystems. HATU and DIPEA were used as coupling reagents. All peptides were blocked at the N-terminus with an acetyl group and at the C-terminus with an amide. The Cys16 residue was substituted with a serine to avoid oligomerization effects. The synthesis were performed using 0.1 mmol of Fmoc-PAL-PEG-PS resin. Stepwise elongation of the peptide chain was accomplished using the extended double-coupling protocol. N-Terminal acetylation was achieved on the peptide resin at the end of the synthesis with acetic anhydride (yields, >99%). An 83.5:2.5:2.5:4:5:2.5 (v/v) TFA/TIS/thioanisole/water/phenol/EDT mixture was used for cleavage. After removal from the resin and deprotection, the cleavage product was precipitated in cold diethyl ether, filtered, dissolved with aqueous TFA buffer, and lyophilized (residues 13−38, 198 mg, 76% yield; W28L, 172 mg, 57% yield; Y25L, 158 mg, 52% yield; Q29S, 182 mg, 60% yield; Q32S, 120 mg, 40% yield). Crude peptides were directly purified by reverse-phase MPLC on a HD-SIL 15−25 μm C18 100 Å preparative column, using a 35 to 82% linear gradient of acetonitrile in 0.08% aqueous TFA (pH 2) for 60 min at a flow rate of 25 mL/min. The purity (>99%) of the peptides was verified on a nucleosil 5 μm C18 300 Å analytical column, using a 40 to 60% linear gradient of acetonitrile in 0.08% aqueous TFA (pH 2) for 20 min at a flow rate of 1 mL/min (residues 13−38, 61 mg, 31% yield; W28L, 44 mg, 26% yield; Y25L, 58 mg, 37% yield; Q29S, 35 mg, 19% yield; Q32S, 26 mg, 22% yield). The peptides were characterized by using positive ion electrospray ionization mass spectrometry [residues 13−38, 3071.56 ± 0.14 (expected, 3071.70); W28L, 2998.18 ± 0.76 (expected, 2998.64); Y25L, 3021.78 ± 0.22 (expected, 3021.68); Q29S, 3030.01 ± 0.45 (expected, 3030.64); Q32S, 3030.32 ± 0.26 (expected, 3030.64)].

NMR Experiments. Samples were prepared using 3 mM PMP1 fragments solubilized in 90:10 H_2O/D_2O solutions containing 120 mM DPC-d_{38} micelles (CIL). The pH value was adjusted to 5. ^{1}H NMR experiments were carried out on 600 and 500 DRX Bruker spectrometers. For the conformational studies, TOCSY and NOESY spectra were recorded at 35 °C with mixing times of 80 and 100−250 ms, respectively. To investigate the peptide−lipid interactions, 12 mM POPS or POPC (Avanti Polar Lipids, Alabaster, AL) was added to the peptide samples in D_2O solutions at pH 5 and 25 °C. Lipid−peptide intermolecular cross-peaks were identified by comparing NOESY spectra in the absence and presence of lipids. Mixing times (t_M) of 100, 300, and 500 ms were used. It is interesting to note that the plateau of the intermolecular NOE buildup curves reaches a t_M value of 500 ms for D_2O solutions but a value of only 150 ms for H_2O solutions. This difference highlights the influence of the interfacial water molecules on the intermolecular spin diffusion effects. Reference NMR spectra of either POPC or POPS solubilized in DPC micelles in the absence of peptide were recorded. The lipid proton assignment was straightforward and found to be consistent with the published data (*21*, *25*).

RESULTS

In a first step, the conformations of the PMP1 fragment (G13−F38) and of its four mutants (Y25L, W28L, Q29S, and Q32S) solubilized in perdeuterated DPC micelles were investigated from NOE and chemical shift data.

Conformation of the PMP1 Fragment and Its Mutants in DPC Micelles. Figure 1A summarizes the sequential and medium-range NOEs involving the backbone protons of the G13−F38 peptide. The intense NH−NH (i, i + 1) NOEs associated with a continuous network of CαH−NH (i, i + 3) and (i, i + 4) contacts indicate the formation of a unique helix from the N-terminus up to Q32. The secondary structure of the G13−F38 peptide is thus in agreement with that previously observed for the shorter fragment, A18−F38 (*8*). Moreover, the ΔδHα profile of the G13−F38 peptide (data not shown) remarkably fits that of the A18−F38 peptide in the C-terminus region extending from Q32 up to F38, which indicates that the average conformation of the cytoplasmic loop is also conserved. As a matter of fact, the major effect of lengthening the peptide sequence from A18−F38 up to G13−F38 is to double the number of residual NH signals observed in a D_2O solution after 1 day, i.e., to significantly

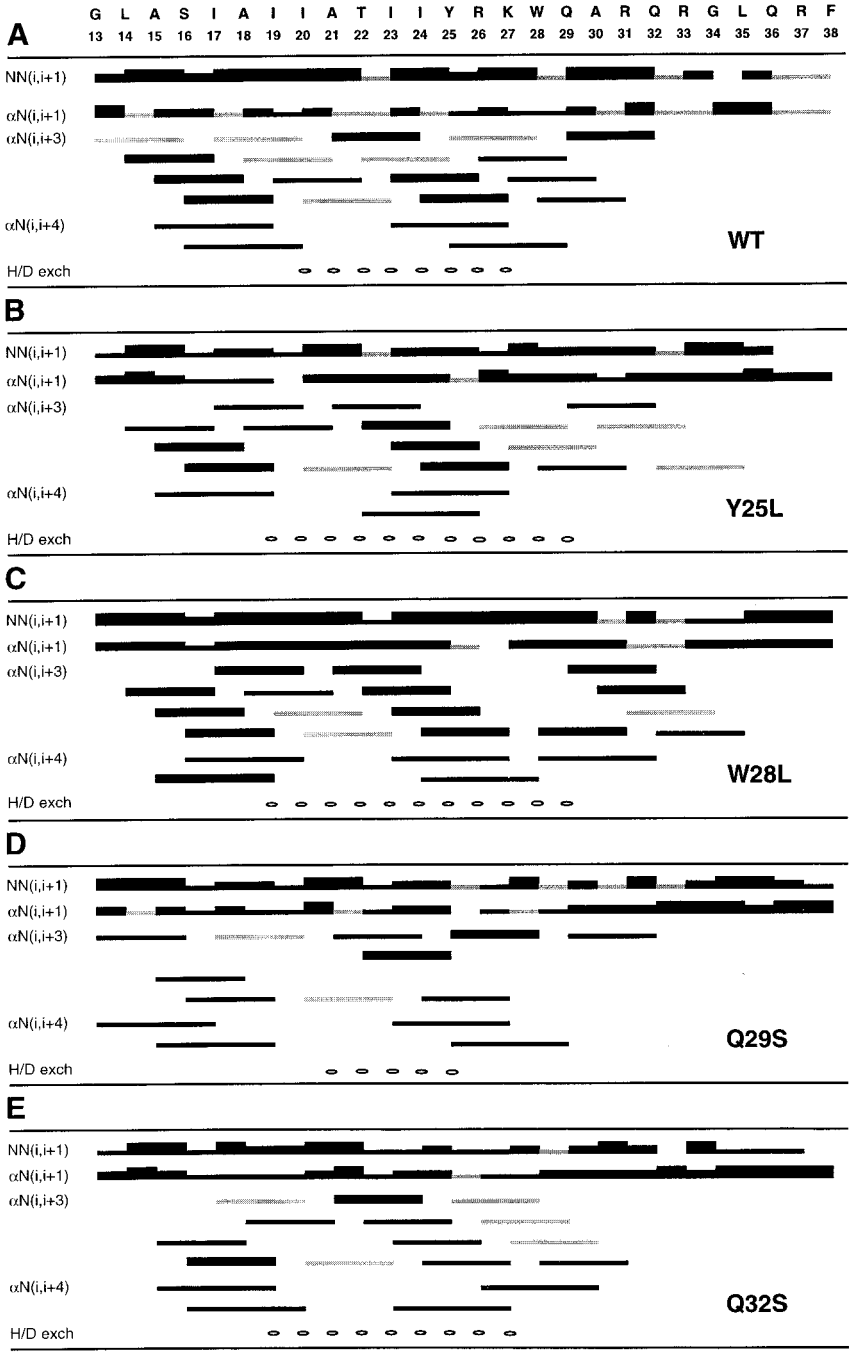

FIGURE 1: Sequential and medium-range NOEs involving the backbone protons of the G13−F38 WT peptide (A) and its four mutants (B−E), solubilized in the presence of perdeuterated DPC micelles at 35 °C and pH 5.0. The bar thickness refers to the NOE intensity (strong, medium, or weak); a gray bar corresponds to an ambiguous NOE. The white symbol (H/D exch) indicates the residue whose NH signal is still detected after 24 h in D_2O solution.

improve the helix stability. The residual NH signals arise from the eight consecutive residues of the I20−K27 segment (Figure 1A).

The NOE networks obtained for the mutants (Figure 1B−E) are roughly close to that of the wild-type (WT) fragment, i.e., characteristic of a unique N-terminal helix. However, significant differences have to be emphasized. First, W28L (Figure 1C) exhibits two additional αN (i, $i + 3$) NOEs involving residues beyond Q32, i.e., A30−R33 and Q32−L35. The effect of the W28 mutation is thus to propagate the helix C-terminus from Q32 up to L35. The NOE data are consistent with the results of the H−D exchange experiment indicating that the W28L mutation extends the sequence segment spanning the protected residues from I20−K27 (Figure 1A) up to I19−Q29 (Figure 1C). In the case of Y25L (Figure 1B), the same increase in the number of residual NH signals is observed but the A30−R33 and Q32−L35 NOEs are ambiguous.

Another point to be emphasized is that the Q29S mutation induces a decrease in the number of (i, $i + 3$) NOEs and of residual NH signals (Figure 1D). This effect can be explained by the less favorable helix propensity of Ser residues as compared to Gln residues (*26*). In the case of Q32S (Figure 1E), as judged by the number of residual NH signals, the

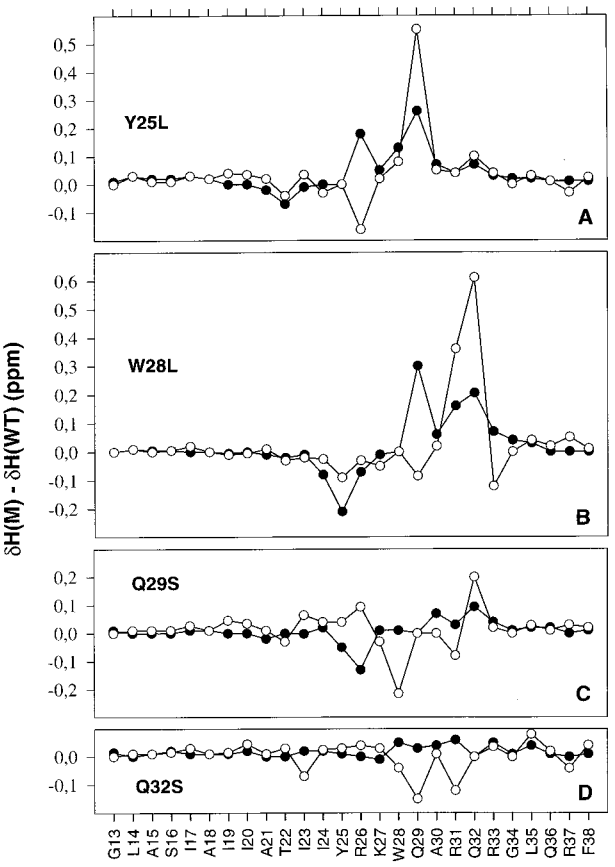

FIGURE 2: Differences in chemical shift, $\Delta\delta H = \delta H\ (M) - \delta H\ (WT)$, observed between the mutated peptides (Y25L, W28L, Q29S, or Q32S) and the wild type (WT), for each residue of the G13−F38 sequence. The black symbols correspond to the Hα chemical shift variation ($\Delta\delta H\alpha$); the white symbols correspond to the largest $\Delta\delta$ value obtained by comparing the chemical shifts of side chain protons ($\Delta\delta$Hsc) for a given residue.

mutational effect is attenuated when compared to that induced by the Q29S mutation. Q32 indeed corresponds to the helix C-terminus, while Q29 is located within the helix.

We have then analyzed the Hα proton chemical shift differences ($\Delta\delta H\alpha$) observed between the WT peptide and each of its mutants (Figure 2, black symbols). The Q32S peptide (Figure 2D) exhibits very weak $\Delta\delta H\alpha$ values, which confirms that its secondary structure is quite close to that of the WT peptide. With regard to Q29S (Figure 2C), $\delta H\alpha$ differences of >0.1 ppm are observed for R26 and Q32, respectively located at the $i - 3$ and $i + 3$ positions with respect to Q29. This is in agreement with a local perturbation of the helix as seen by the NOE and H−D exchange data. In the case of the Y25L and W28L peptides (Figure 2A,B), the $\Delta\delta H\alpha$ values are markedly much larger and affect the I24−G34 region. Taking into account the secondary structure analysis derived from the NOE and H−D exchange data, we may consider that these $\delta H\alpha$ differences mainly reflect the loss of ring current effects. No significant $\delta H\alpha$ variation is observed in the neighboring G13−I23 and L35−F38 segments.

With regard to the side chain protons (Figure 2, white symbols), the most dramatic chemical shift variations concern the NH_2 signals of Q29 and Q32, upon the Y25L and W28L mutations, respectively. The large $\Delta\delta$ values that are observed (∼0.6 ppm) account for the marked side chain to

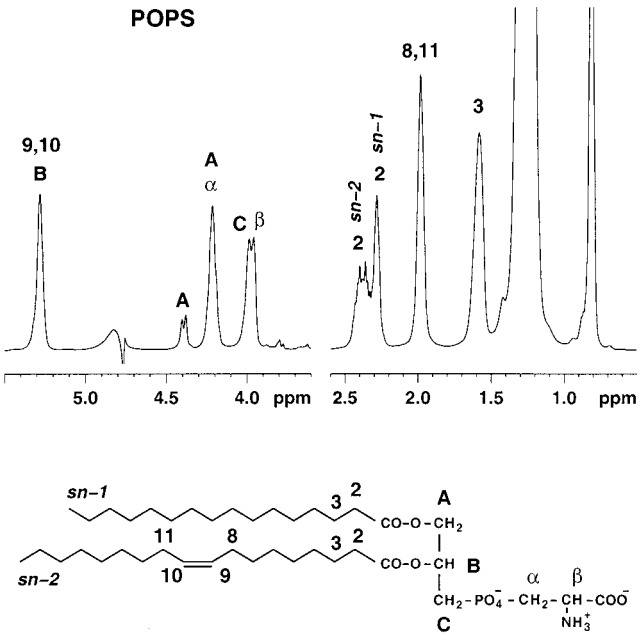

FIGURE 3: ^{1}H NMR spectrum of POPS (12 mM) solubilized in DPC micelles (120 mM) at pH 5 and 25 °C (top trace); the proton numbering of POPS is at the bottom.

side chain stacking that characterizes the Y25−Q29 and W28−Q32 couples in the WT helix. In the case of the W28−Q32 interaction, the intense NOE observed between the aromatic NH proton of W28 and the NH_2 protons of Q32 (data not shown) strongly suggests the existence of an H-bond between the corresponding imino and amide groups.

In a second step, small amounts of either protonated POPC or POPS were cosolubilized with the PMP1 fragments in perdeuterated DPC micelles. The lipid binding properties of the peptides were studied by analyzing the intermolecular NOEs and the chemical shift effects observed on both the peptide and lipid proton signals.

Lipid−PMP1 Fragment Interactions As Seen by Intermolecular NOE Analysis. For the sake of clarity, we briefly describe the set of POPS and POPC resonances before analyzing the intermolecular lipid−peptide NOEs. Figure 3 shows the spectrum of POPS (12 mM) diluted in DPC micelles (120 mM). With regard to the chain protons, it should be noted that the *sn-2* and *sn-1* C2 positions give rise to discernible signals (2.38 and 2.28 ppm, respectively). Upfield are located the resonances of the *sn-2* C8/C11 methylene protons (2 ppm) flanking the double bond, that of the *sn-1/sn-2* C3 protons (1.58 ppm), the broad resonance of the magnetically undifferentiated methylene protons of the acyl chains (1.25 ppm), and, last, the methyl proton signal (0.8 ppm). The *sn-2* C9/C10 CH proton signal overlaps that of the glycerol B proton at 5.3 ppm. The spectrum of POPC in DPC micelles is similar to that of POPS apart from the differences specific to the headgroup structures.

Either POPC or POPS was then cosolubilized with the PMP1 fragments in perdeuterated DPC micelles. The phospholipid concentration was still 12 mM, which corresponds to a lipid to peptide concentration ratio of ∼4. Within the overcrowded aliphatic region of the corresponding NOESY spectrum, detection of unambiguous intermolecular cross-peaks is severely restricted. Fortunately, in the case of PMP1 peptides, NOEs between the peptide ring protons and the

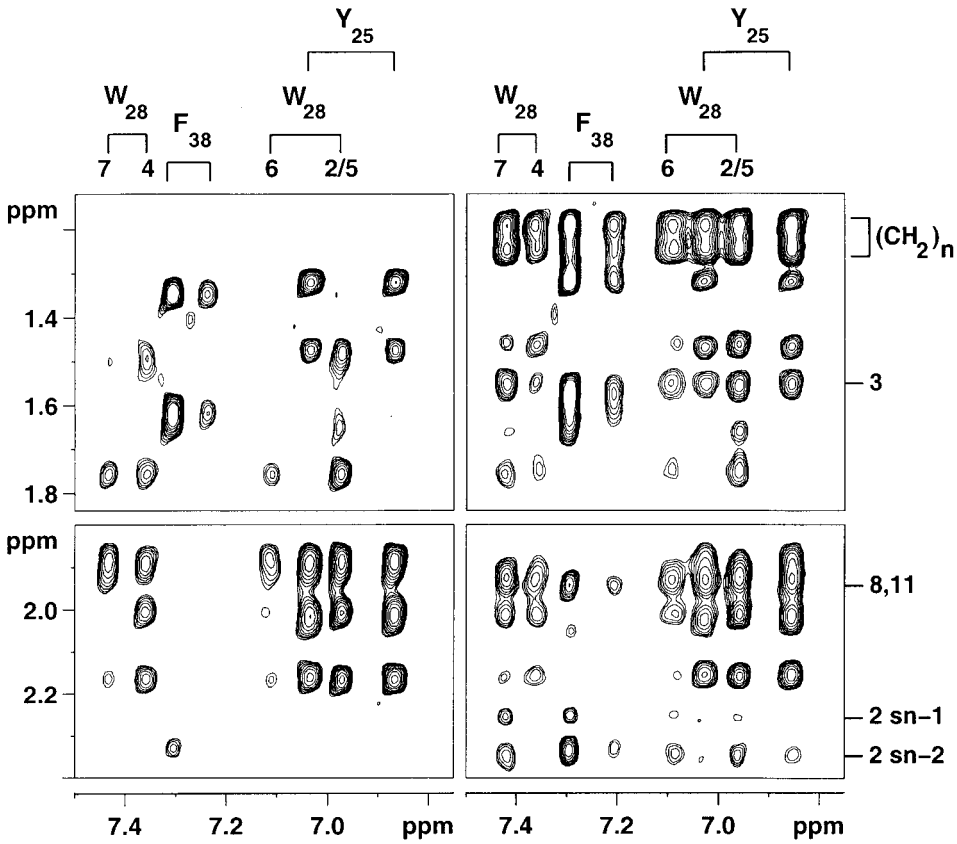

FIGURE 4: Part of a NOESY spectrum (500 ms mixing time) of the G13−F38 peptide (3 mM) solubilized in the presence of DPC micelles (120 mM) in a D_2O buffer at pH 5 and 25 °C, recorded in the absence (left) and presence (right) of POPS (12 mM).

lipid chain protons can be clearly observed from spectra of samples in D_2O solutions. Figure 4 compares the spectrum region containing the NOE cross-peaks between aromatic and aliphatic protons, obtained in the absence (left panel) and presence (right panel) of POPS. The intermolecular NOEs involving the POPS chain protons were thus readily assigned. As far as the glycerophosphoserine protons are concerned, only a few weak intermolecular cross-peaks could be detected, and we did not consider the headgroup region in our NOE analysis. As shown below, the chemical shift data compensate for this lack of information.

Nevertheless, as judged by their number and selectivity, the intermolecular $^1H-^1H$ NOEs arising from the Y25, W28, and F38 signals constitute a relevant data set for satisfactorily probing the location of the PMP1 cytoplasmic domain with respect to the lipids. In particular, Figure 4 shows that (i) for W28 the number and intensity of intermolecular cross-peaks are dramatically larger for H7 than for H4, the former proton being located on the same side of the Trp ring as the NH proton; (ii) the W28 H7 proton contacts both the *sn-1* and *sn-2* C2 protons while the Y25 high-field signal corresponding to the ring H3/H5 protons is only correlated to the *sn-2* C2 one; and (iii) the F38 protons exhibit NOEs with the POPS C8/C11 protons, close to the *sn-2* double bond, which indicates that the F38 ring is deeply buried in the hydrophobic milieu; this result is in agreement with a folding back of the PMP1 C-terminus already observed for the A18−F38 fragment using paramagnetic probes (*9*).

In the presence of POPC (data not shown), we observed an intermolecular NOE network close to that obtained with POPS, as far as the cross-peaks involving Y25 and W28 are concerned. In contrast, the intensity of NOEs arising from F38 was found to be markedly decreased. This difference may account for a specific stabilizing effect exerted by the POPS headgroups on the positioning of the peptide C-terminal region with respect to the lipid chains. We have then analyzed the mutation effects on the intermolecular lipid−peptide NOE network. In the presence of POPC, no significant difference was observed when the WT peptide was replaced with any of the four mutants, i.e., Y25L, W28L, Q29S, or Q32S. In the case of POPS, while the Y25L and Q29S mutations have still no effect, the W28L and Q32S mutations markedly decrease the intensity of the NOEs involving F38. Therefore, the W28L and Q32S mutations tend to abolish the specific stabilizing effect exerted by the POPS polar heads.

Lipid−PMP1 Fragment Interactions As Seen by the Chemical Shift Variations of the Peptide Protons. Upon addition of either POPS or POPC, several peptide resonances undergo a detectable shift, which provides complementary insight into the lipid−peptide interaction network. Most of these shifts concern the polar side chains of the PMP1 cytoplasmic domain. Figure 5A displays, for a given side chain, the largest chemical shift variation ($\Delta\delta$Hsc) obtained for the WT PMP1 fragment upon addition of POPS (black bars) and POPC (white bars). For both lipids, $\Delta\delta$Hsc values of >0.02 ppm are observed for R26, R31, and R37. However, the variation observed for R31 in the presence of POPS is 2 times larger than that obtained with POPC. Furthermore, the sign and amplitude of the Q32 δHsc variation appear to be specific to the POPS effect.

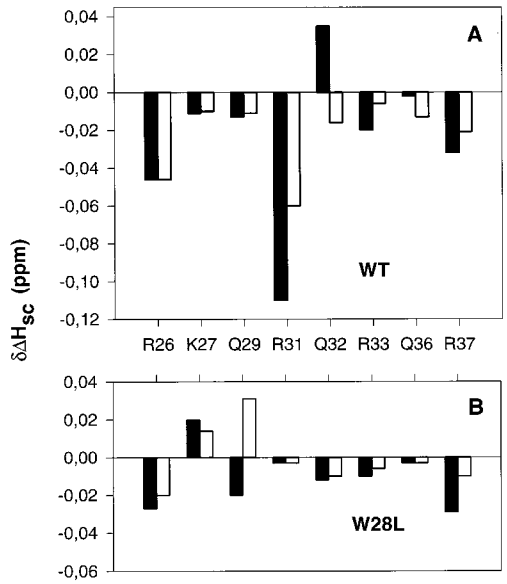

FIGURE 5: Largest ^{1}H chemical shift variation ($\Delta\delta$Hsc) observed for each of the polar side chains of the PMP1 cytoplasmic domains upon addition of POPS (black bars) and POPC (white bars): (A) WT and (B) W28L peptide. The experimental conditions are those given in the legend of Figure 4.

Analysis of the chemical shift data of the mutants in the presence of either POPS or POPC does not provide any significant supplementary information, except for W28L. Figure 5B shows that, with the W28L mutation, the $\Delta\delta$Hsc value of R31 becomes null in the presence of either POPC or POPS and that of Q32 in the presence of POPS is inverted and severely reduced. Therefore, as in the case of the NOE data, the W28L mutation tends to abolish the chemical shift effects distinguishing POPC and POPS in the presence of the WT peptide.

Lipid−PMP1 Fragment Interactions As Seen by the Chemical Shift Variations of the Lipid Protons. The upper trace of Figure 6 shows the low-field region of the NMR spectra of POPS (left panel) and POPC (right panel) in the absence of peptide. The displayed region contains most of the signals of the glycerol and polar headgroup protons and that of the *sn-2* C9/C10 CH protons overlapping the glycerol B one at 5.3 ppm. The lower traces show the same spectrum region in the presence of the WT peptide and its four mutants.

Whereas addition of either the WT peptide or its mutants does not affect the POPC signals, significant variations are observed in the POPS spectrum. These changes are thus specific to the polar head structure. First, addition of the WT peptide induces a high-field shift of one of the signals forming the unresolved peak located at 5.3 ppm. The shifted resonance exhibits an intense cross-peak with the C8/C11 signal (located at 2 ppm) and therefore corresponds to the C9/C10 protons (Figure 6). This result can be related to the intermolecular NOE analysis showing that the main difference observed when passing from POPS to POPC is the intensity loss of the acyl chain−F38 ring contacts. We may thus assign the shift of the C9/C10 signal specifically observed in the presence of POPS to a F38 ring current effect. As previously mentioned, the POPS headgroups most probably stabilize the positioning of the peptide C-terminal region with respect to the lipid chains. The second characteristic POPS shifts observed upon addition of the WT peptide

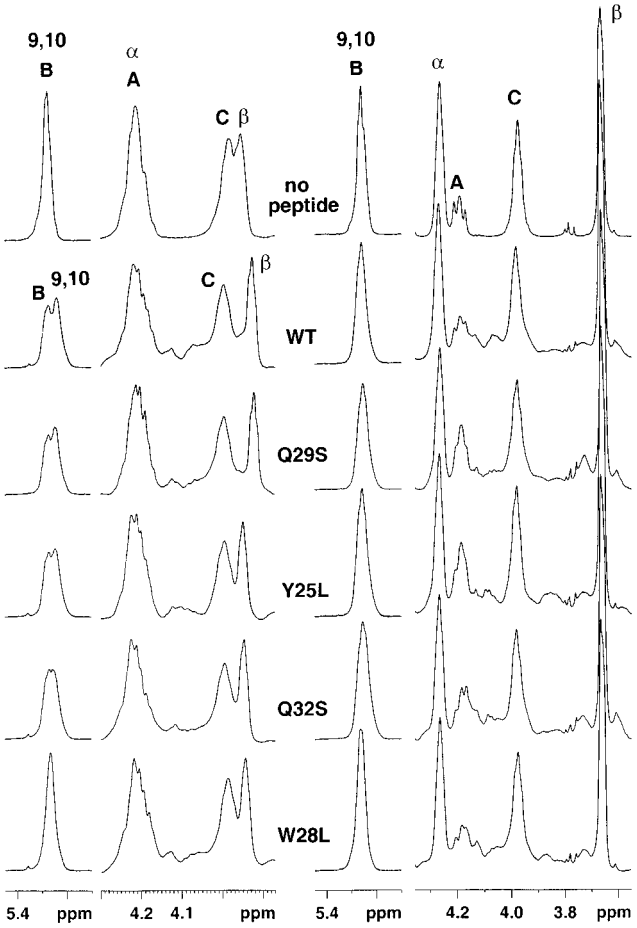

FIGURE 6: Low-field part of the ^{1}H NMR spectra of POPS (left) and POPC (right) solubilized in DPC in the absence (top trace) and presence of the WT peptide and its four mutants. The experimental conditions are those given in the legend of Figure 4.

concern the resonances of the serine CHβ proton and of the glycerol C protons (Figure 6). To a lesser extent, the serine $CH_2\alpha$ signal (only detectable in two-dimensional spectra) is also shifted in the presence of the WT peptide. Besides, the glycerol C resonance corresponds to the methylene protons closest to the phosphate group (Figure 3). These perturbations thus directly reflect the specific involvement of the POPS headgroups in the peptide−lipid interactions.

In the presence of the Q29S mutant, all the specific shifts are still observed (Figure 6). In contrast, with the Y25L and Q32S mutations, the serine β resonance recovers its value initially observed in the absence of peptide while, in parallel, the C and C9/C10 protons undergo a shift smaller than that induced by the WT peptide. Last, the W28L mutation (bottom trace in Figure 6) almost fully abolishes the specific shifts of the POPS protons, observed in the presence of the WT peptide.

DISCUSSION

The lipid species used in this study share a common structural motif comprising the acyl chains, the glycerol backbone, and the phosphate group. They only differ in their polar head, either a choline or a serine group. This obvious observation emphasizes a general result of our study that will guide the discussion: when the PMP1 fragment is diluted in micelles with small amounts of either POPC or POPS,

the NMR data which probe the lipid binding interactions reflect both specific and common features.

The specificity for the PS species is revealed by the following results. (i) The serine resonances but not those of the choline group are sensitive to the presence of the PMP1 fragments. (ii) The serine response is reciprocated by a specific change in the Q32 signals. (iii) The implication of Q32 in the PMP1−POPS interaction network is confirmed by the Q32S mutation that removes the POPS headgroup response. Besides, the specific shift of the POPS *sn-2* C9/C10 proton resonance associated with the presence of intense acyl chain−F38 ring NOEs indicates that the POPS headgroups stabilize the positioning of the peptide C-terminal region with respect to the lipid chains. A second set of NMR data highlights lipid−peptide interactions common to both POPS and POPC: (i) the chemical shifts of the arginine side chains, although the presence of POPS generally induces effects markedly greater than those obtained for POPC, especially in the case of R31; and (ii) the acyl chain−Y25 ring NOEs and the acyl chain−W28 ring NOEs.

The W28L mutation markedly affects both specific and nonspecific aspects of the lipid binding properties of the PMP1 fragment. The specificity for POPS is markedly perturbed as judged by the POPS headgroup and Q32 side chain resonances that tend to recover their initial chemical shifts. The loss of specificity is also reflected by the absence of the POPS *sn-2* C9/C10 shift associated with a marked decrease in the magnitudes of the intermolecular NOEs involving F38. The nonspecific perturbing aspect of the W28L mutation is probed by the absence of the R31 characteristic shift upon addition of either POPC or POPS.

The effects of the W28L mutation on the lipid binding properties can be readily related to concomitant conformational perturbations: (i) the Q32 side chain that directly contributes to the specificity for POPS, loses its H-bond partner, the indole NH of W28, and (ii) the helix C-terminus residue becomes L35 instead of Q32. Conversely, in the case of the WT peptide, W28 ensures the adequate interfacial conformation of the cytoplasmic domain and its interaction with Q32 induces the appropriate positioning of the glutamine amide group for an optimized interaction with the POPS serine group as proposed in Figure 7A. Besides, R31 appears to be the most suitable candidate for interacting with the POPS phosphate group, which completes the lipid−peptide electrostatic interaction network. The major result of our study is therefore to reveal the concerted influence of a tryptophan, W28, and a glutamine residue, Q32, on the interfacial conformation and lipid binding specificity of the PMP1 cytoplasmic domain.

The mutation of the other aromatic residue of the helix, Y25L, affects the binding of POPS as judged by the variation of the PS headgroup chemical shifts. However, the characteristic shift of the POPS *sn-2* C9/C10 resonance is still observed as well as those of R31 and Q32. As shown by our conformational data, Y25 is implied in the interfacial location of the WT PMP1 cytoplasmic domain through the Y_{25}-R-K-W_{28} amphiphilic motif, and therefore, its mutation partially destabilizes the interaction network, ensuring the lipid binding specificity. Last, the Q29S mutation does not exert any direct influence on the lipid binding properties of the PMP1 fragment.

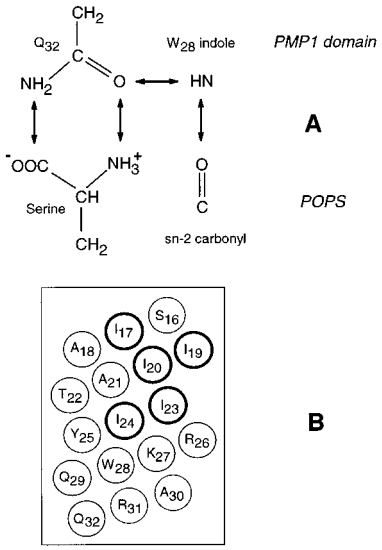

FIGURE 7: (A) Possible interaction network involving W28, Q32, and POPS. (B) Schematic representation of the L14−Q32 helix segment of PMP1.

We then used the constraints derived from the intermolecular NOEs involving Y25 and W28 to map the hydrophobic contacts between the lipid acyl chains and the peptide helix core. A simple docking procedure between one POPS molecule and the G13−Q32 helix shows that the POPS *sn-2* oleoyl chain partly lies in a groove formed on one side of the helix. This groove results from the marked inhomogeneous distribution of the hydrophobic surface area around the I17−Y25 helix segment as illustrated in Figure 7B: one side contains the Y25 aromatic residue and three short side chain residues, i.e., A18, A21, and T22, while the opposite side exposes five long and β-branched hydrophobic side chains, i.e., I17, I19, I20, I23, and I24. As a result, the I17−Y25 segment of the helix rod exhibits a marked concavity into which a part of the POPS *sn-2* oleyl chain inserts. Besides, our solid-state ^{2}H NMR study of PMP1 fragments in mixed POPS/POPC bilayers (*10*) showed that each peptide selectively binds to eight POPS molecules. We may therefore assign a specific role to one of the POPS molecules: its *sn-2* chain inserts into the groove drawn along one side of the PMP1 helix, while its serine group directly interacts with the Q32 side chain and its phosphate group with R31. The appropriate interfacial positioning of the Q32 amide group is ensured by the W28−Q32 interaction. The resulting POPS−PMP1 association constitutes a stabilized framework for binding other POPS molecules. The binding of anionic phospholipids around this framework is of course favored by the ringlike interfacial distribution of the five basic side chains and the ability of one arginine residue to form salt bridges with two phosphoserine groups. Interestingly, from a recent crystallographic structure of the factor V C2 domain (*27*), it has been suggested that a glutamine residue (Q48) would play a prominent role in the PS binding specificity of this C2 domain.

REFERENCES

1. McAuley, K. E., Fyfe, P. K., Ridge, J. P., Isaacs, N. W., Cogdell, R. J., and Jones, M. R. (1999) *Proc. Natl. Acad. Sci. U.S.A. 96*, 14706−14711.
2. Belrhali, H., Nollert, P., Royant, A., Menzel, C., Rosenbusch,

J. P., Landau, E. M., and Pebay-Peyroula, E. (1999) *Structure 7*, 909−917.
3. Luecke, H., Schobert, B., Richter, H. T., Cartailler, J. P., and Lanyi, J. K. (1999) *J. Mol. Biol. 291*, 899−911.
4. Essen, L. O., Soegert, W. D., Lehmann, W. D., and Oesterhelt, D. (1998) *Proc. Natl. Acad. Sci. U.S.A. 95*, 11673−11678.
5. Tsukihara, T., Aoyama, H., Yamashita, E., Tomizaki, T., Yamaguchi, H., Shinzawa-Itoh, K., Nakashima, R., Yaono, R., and Yoshikawa, S. (1996) *Science 272*, 1136−1144.
6. Navarre, C., Ghislain, M., Leterme, S., Ferroud, C., Dufour, J.-P., and Goffeau, A. (1992) *J. Biol. Chem. 267*, 6425−6428.
7. Navarre, C., Catty, P., Leterme, S., Dietrich, F., and Goffeau, A. (1994) *J. Biol. Chem. 269*, 21262−21268.
8. Beswick, V., Roux, M., Navarre, C., Coïc, Y. M., Huynh-Dinh, T., Goffeau, A., Sanson, A., and Neumann, J. M. (1998) *Biochimie 80*, 451−459.
9. Beswick, V., Guerois, R., Ochsenbein, F., Coïc, Y. M., Huynh-Dinh, T., Tostain, J., Noël, J. P., Sanson, A., and Neumann, J. M. (1998) *Eur. Biophys. J. 28*, 48−58.
10. Roux, M., Beswick, V., Coïc, Y. M., Huynh-Dinh, T., Sanson, A., and Neumann, J. M. (2000) *Biophys. J. 79*, 2624−2631.
11. Killian, J. A., and Von Heijne, G. (2000) *Trends Biochem. Sci. 25*, 429−434.
12. White, S., and Wimley, W. C. (1999) *Annu. Rev. Biophys. Biomol. Struct. 28*, 319−365.
13. Yuen, C. T. K., Davidson, A. R., and Deber, C. M. (2000) *Biochemistry 39*, 16155−16162.
14. Lauterwein, J., Bösch, C., Brown, L. R., and Wüthrich, K. (1979) *Biochim. Biophys. Acta 556*, 244−264.
15. Baleja, J. D. (2001) *Anal. Biochem. 288*, 1−15.
16. MacKenzie, K. R., Prestegard, J. H., and Engelman, D. M. (1997) *Science 276*, 131−133.
17. Soulié, S., Neumann, J. M., Berthomieu, C., Moller, J. V., Le Maire, M., and Forge, V. (1999) *Biochemistry 38*, 5813−5821.
18. Kutateladze, T., and Overduin, M. (2001) *Science 291*, 1793−1796.
19. Arora, A., Abildgaard, F., Bushweller, J. H., and Tamm, L. K. (2001) *Nat. Struct. Biol. 8*, 334−338.
20. Giragossian, C., and Mierke, D. F. (2001) *Biochemistry 40*, 3804−3809.
21. Neumann, J. M., Zachowski, A., Tran-Dinh, S., and Devaux, P. F. (1985) *Eur. Biophys. J. 11*, 219−223.
22. Carpino, L. A., and Han, G. Y. (1972) *J. Org. Chem. 37*, 3404−3409.
23. Atherton, E., Fox, H., Harkiss, D., and Sheppard, R. C. (1978) *J. Chem. Soc., Chem. Commun. 76*, 539−540.
24. Chang, C.-D., and Meienhofer, J. (1978) *Int. J. Pept. Protein Res. 11*, 246−249.
25. Sanson, A., Monck, M. A., and Neumann, J. M. (1995) *Biochemistry 34*, 5938−5944.
26. Pace, C. N., and Sholtz, J. M. (1998) *Biophys. J. 75*, 422−427.
27. Macedo-Ribeiro, S., Bode, W., Huber, R., Quinn-Allen, M., Kim, S. W., Ortel, T., Bourenkov, G. P., Bartunik, H. D., Stubbs, M. T., Kane, W. H., and Fuentes-Prior, P. (1999) *Nature 402*, 434−439.

BI010924E